Towards the Mullitization of Mullite Precursor Gel Synthesised from Kaolin Derived-Sodium Metasilicate and Sodium Aluminate

A. C. K. Amuzu^{1*}; A. Abandoh¹; B. Puzer¹; F. J. K. Adzabe²; S. Anane³; L. K. Labik¹; I. Nkrumah¹; E. K. K. Abavare¹; B. Kwakye-Awuah¹

¹Department of Physics, Kwame Nkrumah University of Science and Technology, Kumasi, Ghana.

²Department of Mechanical Engineering, Kumasi Technical University, Kumasi, Ghana.

³Department of Programs, Ghana Investment for Electronic Communications, Kumasi, Ghana.

Corresponding Author: A. C. K. Amuzu^{1*}

Publication Date: 2025/10/30

Abstract: A novel synthesis technique was developed for producing mullite nanopowder from kaolinite clay. Kaolin was converted to metakaolin, reduced into sodium silicate and aluminate, and reassembled at the molecular level through controlled precipitation to form an aluminosilicate hydrogel with intentionally high aluminum content. The hydrogel was sintered at 950, 1050, and 1150 °C for 30 min. X-ray Fluorescence spectroscopy (XRF) confirmed enrichment in alumina, while Fourier Transform Infrared spectroscopy (FTIR) revealed progressive dehydroxylation and the emergence of mullite-specific bonds. X-ray Diffraction (XRD) indicated the onset of mullite crystallization at 950 °C and nearly complete transformation at 1150 °C, achieving ~99 % phase purity. Scanning Electron Microscopy (SEM) showed a clear morphological evolution from porous, amorphous gel particles to faceted grains at 950 °C, and well-interlocked mullite grains (2–4 μ m) with minimal porosity at 1150 °C. Energy Dispersive X-ray spectroscopy (EDX) confirmed the elemental progression toward the theoretical Al/Si ratio for stoichiometric mullite. These findings demonstrate that mullite nanopowder with high phase purity and desirable microstructural features can be synthesized at 1150 °C from kaolin.

Keywords: Kaolin, Metakaoln, Gel, Mullite, Stoichiometric.

How to Cite: A. C. K. Amuzu; A. Abandoh; B. Puzer; F. J. K. Adzabe; S. Anane; L. K. Labik; I. Nkrumah; E. K. K. Abavare; B. Kwakye-Awuah (2025). Towards the Mullitization of Mullite Precursor Gel Synthesised from Kaolin Derived-Sodium Metasilicate and Sodium Aluminate. *International Journal of Innovative Science and Research Technology*, 10(9), 3075-3083. https://doi.org/10.38124/ijisrt/25sep1144

I. INTRODUCTION

Mullite (3Al₂O₃•2SiO₂) is an aluminosilicate structural material valued for its unique combination of properties, including low thermal expansion, excellent thermal shock resistance, high refractoriness, good creep resistance, and chemical inertness [1,2,3,4, 5]. These attributes have led to its widespread use in structural ceramics, refractory materials, and electronic substrates, as well as in advanced applications such as aerospace components and ceramic matrix composites [3,6].

Despite its technological importance, the synthesis of phase-pure mullite remains a subject of continuing research, as its formation depends strongly on the choice of raw materials, precursor homogeneity, and processing route [3,7,8,9]. Several methods have been employed to synthesize mullite, including solid-state reaction, hydrothermal

synthesis, mechanical activation, and chemical routes such as sol-gel and precipitation [7,8,10,11]. Among these, solid-state reactions from natural raw materials such as sillimanite, andalusite, kyanite, bauxite, or kaolinite are the most widely practiced due to the availability and low cost of these minerals [12]. However, such methods typically require calcination at temperatures above 1400 °C for complete mullitization, and they often yield multiphase products with residual glassy phases due to poor mixing of silica and alumina at the particle level [3,11]. These shortcomings result in high energy demands and limit the structural homogeneity of the final mullite.

In contrast, chemical methods such as sol-gel, precipitation, and hydrolysis enable molecular-level mixing of Al^{3+} and Si^{4+} species, which significantly lowers the mullitization temperature to below 1200 °C and improves phase purity [8,10,13]. However, these methods typically rely

https://doi.org/10.38124/ijisrt/25sep1144

on costly precursors such as tetraethyl orthosilicate (TEOS), tetramethyl orthosilicate (TMOS), silicic acid, or inorganic aluminum salts, making them less suitable for large-scale and cost-sensitive applications.

To overcome these challenges, recent research has focused on developing hybrid approaches that combine the cost-effectiveness of natural raw materials with the advantages of molecular-level precursor mixing. In particular, kaolinite a widely available clay mineral has attracted attention as a potential precursor for mullite synthesis due to its suitable alumina-to-silica ratio and abundance. Conventionally, kaolin is thermally activated to metakaolin and then processed via solid-state reaction, but this still suffers from high temperature requirements and incomplete phase conversion [14,15,16, 17].

The present study introduces a novel approach that chemically converts kaolin into sodium metasilicate and sodium aluminate, which are then recombined under controlled conditions to form a homogeneous mullite precursor gel. Unlike previously reported solid-state routes from kaolin, this method ensures molecular-level mixing of silica and alumina while maintaining the economic advantage of a natural raw material feedstock. This integrated approach is expected to lower the mullitization temperature, enhance phase purity, and improve microstructural homogeneity, thereby reducing energy consumption relative to conventional kaolin-based processes.

Accordingly, the aim of this work is to synthesize mullite precursor gel from kaolin-derived sodium metasilicate and sodium aluminate via controlled precipitation and to investigate its structural evolution during calcination using XRD, FTIR, SEM, and EDX. This study provides new insights into the mullitization of kaolin-derived precursor gels and establishes a cost-effective and scalable pathway for high-purity mullite synthesis.

II. MATERIALS AND METHODS

➤ Materials

The main precursor kaolinite clay, obtained from Teleku-Bokazo in the Western region of Ghana, was thoroughly beneficiated and characterized for its chemical composition. Chemical reagents employed include Sodium hydroxide (NaOH) pellets (99 wt% purity), Oxalic acid 99 wt%) and ammonia (98 wt%) procured from Analar Normapur, UK, sulphuric acid (H₂SO₄, 95 wt%), and Whatman filter paper (No. 1) were obtained from Sigma-Aldrich, Germany. The chemical reagents were of analytical grade and were used as received without further purification.

➤ Methods

• Preparation of Sodium Aluminate and Silicate

A known mass of the beneficiated kaolin was calcined at 850 °C for 30 min to produce an amorphous reactive phase known as metakaolin. The metakaolin was completely dealuminated using sulphuric acid to obtain aluminum sulphate which was used to prepare 1 M aqueous sodium

aluminate solution with alumina concentration of 35 %. The silica-rich residue was thoroughly washed, leached hydrothermally with sodium hydroxide at 140 °C and vacuum filtered to obtain a clear, residue-free sodium silicate solution with a silica content of approximately 28.0%. This solution was stored in a sealed container for subsequent use.

• Formation Mullite Gel and Crystalline Mullite Nano-Powder

Mullite was synthesized based on the stoichiometric molar ratio of 3:2 (Al₂O₃:SiO₂). To prepare the precursor gel, corresponding weights of sodium aluminate and sodium silicate solutions were measured according to this ratio and transferred into separate glass beakers. The sodium silicate solution was first diluted with distilled water and stirred at 90 rpm under ambient conditions for a predetermined duration. Subsequently, the sodium aluminate solution was also diluted and added dropwise to the sodium silicate solution while stirring continued. As the addition progressed, gel formation was initiated. At this point, the stirring speed was increased to 120 rpm and maintained for one hour to ensure uniform mixing and gel formation. The pH of the gel was then adjusted to neutrality under continued stirring. After reaching a stable neutral pH, the gel was stirred for an additional 30 minutes to complete the reaction process. The resulting gel was vacuum filtered, thoroughly washed with distilled water, dried, ground into fine powder, and stored in a sealed plastic bag. To study the evolution of the crystalline mullite phase, portions of the gel were calcined in a muffle furnace at 950, 1050 and 1150 °C. A constant heating rate of 2 °C/min and a holding time of 30 minutes were applied across all temperature settings. A flow chart summarizing the entire synthesis procedure is presented in Fig. 2.1. The key chemical reactions involved in the formation of mullite gel and its subsequent crystallization are illustrated in Equations (1) and (2).

$$6 \text{NaAlO}_{2 \text{ (aq)}} + 2 \text{Na}_2 \text{SiO}_{3 \text{ (aq)}} + 4 \text{H}_2 \text{O} \rightarrow \text{Al}_6 \text{Si}_2 \text{O}_{13} \cdot \text{xH}_2 \text{O}_{(8)} + 10 \text{NaOH}_{(aq)} \tag{1}$$

$$Al_6Si_2O_{13} \cdot xH_2O_{(8)} \xrightarrow{\Delta} Al_6Si_2O_{13 (8)} + xH_2O_{(8)} \uparrow$$
 (2)

III. CHARACTERIZATION TECHNIQUES

The beneficiated kaolin, metakaolin and the assynthesized gel were analyzed quantitatively for its chemical composition using X-ray Fluorescence (XRF, Rigaku NEX CG). The mineralogical properties of the gel and the derivative mullite samples were analysed using X-ray diffractometer (EMPYREAN) equipped with a Cu-ka radiation of wavelength 1.5406 Å. Scanning of the samples were done at a step size of $2\theta = 0.105^{\circ}$ in a range of 5 to 85° at a scanning rate of 1°/min. The device operated at 40 mA and 45 kV for phase analysis using the Bragg – Brentano geometry. Scanning electron microscopy (SEM, Hitachi S4800, Japan) equipped with nominal electron beam voltages of 15 kV, was used to examine the morphologies of the gel and the mullite samples. Fourier Transform Infrared (FTIR) spectroscopy (Perkin-Elmer Spectrum 100) was employed to analyze the functional groups of the samples. Spectra were

https://doi.org/10.38124/ijisrt/25sep1144

acquired by averaging 100 scans at a resolution of 4 cm⁻¹ over the mid-infrared region (4000–400 cm⁻¹), expressed in % transmittance (%T). A background air spectrum was

recorded prior to sample measurement to correct for atmospheric interferences.

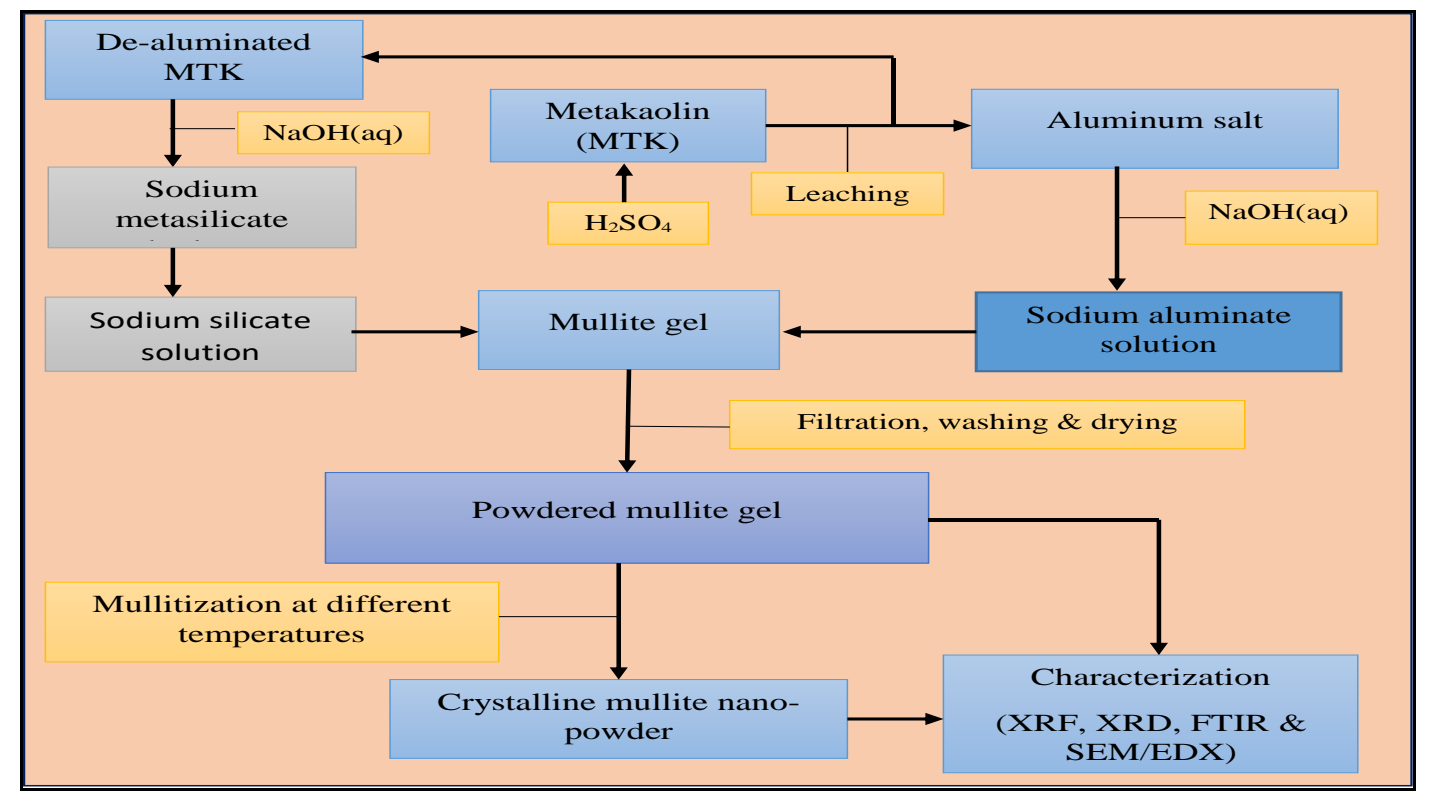


Fig 1 Schematic Representation of the Synthesis Route of Mullite from Kaolinite Clay

IV. RESULTS AND DISCUSSIONS

Chemical compositions of the beneficiated kaolin and metakaolin determined by XRF are summarized in Table 1. The beneficiated kaolin contained 52.34 wt% SiO_2 and 30.53 wt% Al_2O_3 , indicating its suitability as an aluminosilicate source. Minor oxides such as Fe_2O_3 (4.76 wt%), K_2O (1.96 wt%), CaO (2.55 wt%), and Na_2O (2.54 wt%) were also present, while the loss on ignition (LOI) was 3.98 wt%, consistent with structurally bound hydroxyl groups. Calcination significantly reduced the LOI to 1.25 wt%,

confirming effective dehydroxylation and formation of reactive metakaolin. This transformation increased the relative Al_2O_3 content (34.65 wt%) and rendered the material highly reactive suitable for dealumination [18, 19]. The chemical composition of the synthesized mullite precursor gel derived from kaolin-based sodium aluminate and sodium silicate is summarized in Table 1. The gel exhibited a composition predominantly comprising silica (SiO₂) and alumina (Al_2O_3), consistent with the stoichiometric requirement for mullite formation [7, 16].

Table 1 Chemical Compositions of Beneficiated and Calcined (Metakaolin) Kaolin

Sample	Chemical Composition wt%										
	SiO ₂	Al ₂ O ₃	Fe ₂ O ₃	SO ₃	Na ₂ O	K ₂ O	CaO	PbO	ZrO	Others	LOI
Beneficiated kaolin	52.34	30.53	4.76	ND	2.54	1.96	2.55	0.69	0.50	0.55	3.98
Metakaolin	51.52	34.65	4.45	ND	2.52	1.34	2.25	0.68	0.51	0.53	1.25
Mullite Gel	22.86	69.84	ND	2.15	2.58	0.00	ND	ND	0.01	0.57	0.01

The SiO₂ and Al₂O₃ contents collectively accounted for the majority of the gel mass, confirming the effectiveness of the precursor preparation route in achieving a silica–alumina system closed to the mullite stoichiometry (3Al₂O₃•2SiO₂). Minor constituents, including Na₂O, Fe₂O₃, and trace oxides such as K₂O, CaO, and ZrO₂, were also detected, which could be attributed to residual sodium from the alkaline solutions used for the gel preparation, inherent iron oxides and naturally occurring mineral impurities from the kaolin.

These impurities were present in very low concentrations, minimizing their potential interference with mullitization. In particular, the low Fe_2O_3 content was significant because excessive iron could promote the formation of secondary glassy phases and which could affect mullite crystallinity. The overall composition of the gel has shown a favorable alumina-to-silica ratio, tailored to offset glassy phase formation and promote mullite crystallization at relatively lower temperatures [3]. This result corroborated the intended

design of the synthesis process, where controlled precipitation ensured molecular-level homogeneity of the precursors, thereby enhancing the reactivity and reducing the activation energy for mullite formation during sintering.

Comparable studies have reported similar compositional trends for optimized mullite precursors synthesized via sol—gel or chemical precipitation techniques [10, 20]. Thus, the composition of the gel obtained in this work provides a strong basis for achieving phase-pure mullite with minimal secondary phases during thermal treatment.

The FTIR spectra of the as-synthesized mullite gel and its corresponding products obtained after thermal treatment at sintering temperatures of 950, 1050, and 1150 °C are presented in Figure 1. The spectrum of the precursor gel was

characterized by a broad band centered around 3397 cm⁻¹, attributed to the O-H stretching vibrations of adsorbed or bound water molecules, and a shoulder observed at 1650 cm⁻¹ corresponding to bending vibration (δ-OH) of water, confirming the hydrated nature of the gel. In the lower wavenumber region (1200-400 cm⁻¹), several broad but, discernible absorption bands were identified at 1140, 950, 690, 535, and 420 cm⁻¹. These bands are commonly assigned to asymmetric stretching of Si-O-Al linkages, Al-O and Si-O bending vibrations, and framework deformations associated with disordered alumino-silicate networks [14, 20]. Upon thermal treatment at 950 °C, the FTIR spectrum exhibited notable changes. The disappearance of the O-H stretching and bending bands confirmed the elimination of physically and chemically bound water.

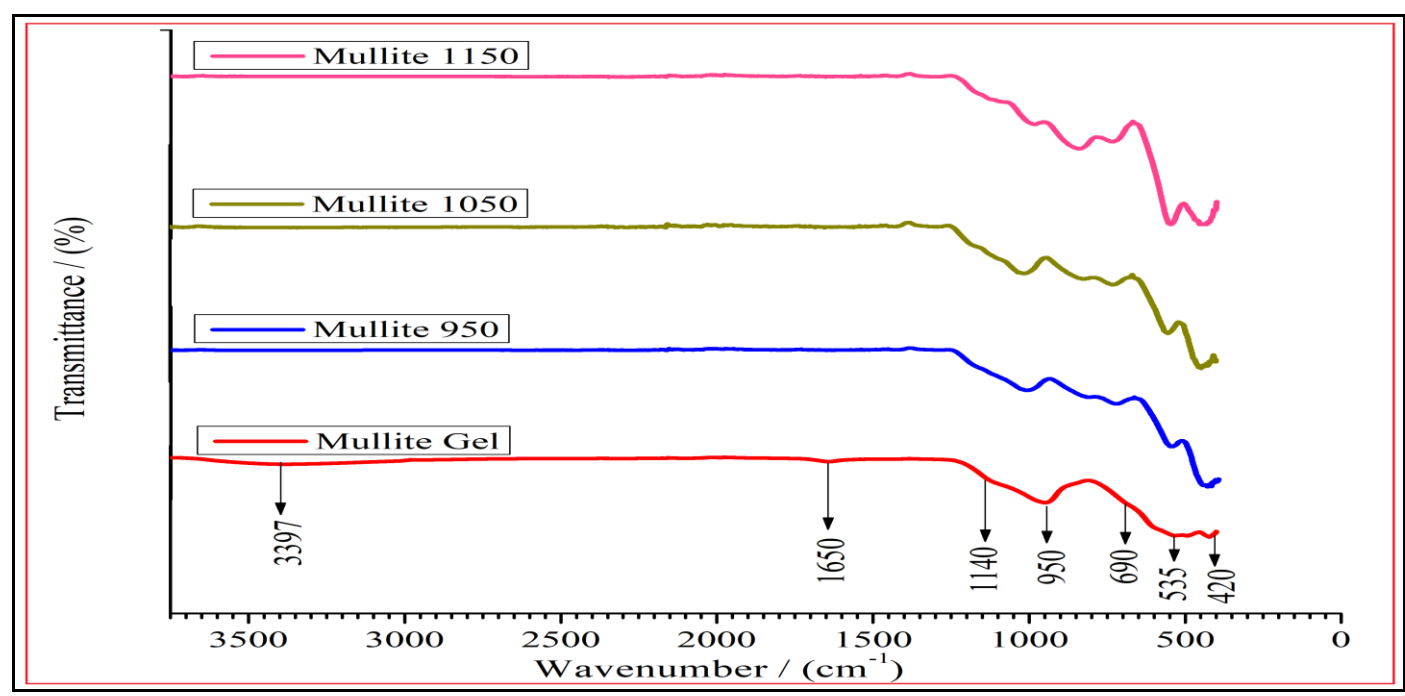


Fig 2 FTIR Spectral of Mullite Gel and Sintered Mullite

Simultaneously, a more pronounced absorption at 950 cm⁻¹ and increased resolution of the bands at 690 and 535 cm⁻¹ indicated the onset of structural reorganization and formation of intermediate alumino-silicate frameworks with increased short-range order. The sample treated at 1050 °C displayed a further sharpening and slight shift of the Si-O-Al stretching band toward ~1020 cm⁻¹, alongside a more defined presence of the Al-O vibration at ~535 cm⁻¹. These spectral changes suggested a continued structural consolidation and polymerization, indicating the nucleation of mullite crystallites within the evolving matrix. At the highest sintering temperature of 1150 °C, the FTIR spectrum was dominated by well-resolved peaks centered around 1100, 690, 535, and 420 cm⁻¹. These sharp absorptions are characteristic of the crystalline mullite phase, especially the strong bands in the 500-600 cm⁻¹ region, which correspond to Al-O stretching in octahedral coordination (AlO₆) [20]. The spectral features at this stage confirmed the successful transformation of the amorphous gel into crystalline mullite (3Al₂O₃·2SiO₂), consistent with XRD results presented in Figure 3.2. Furthermore, the FTIR analysis provided direct evidence of the structural evolution from a hydrated and amorphous alumino-silicate gel to a well-crystallized mullite phase through thermal treatment [21, 22]. The progressive disappearance of hydrous features and the emergence of characteristic mullite bands with increasing temperature corroborated the crystallization behavior observed in XRD, and further validated the effective conversion of the kaolin-based gel precursor into mullite at relatively low temperature.

The XRD patterns of mullite gel and its sintered products presented in Figure 3 revealed distinct phase evolution in response to increasing sintering temperature. In the as-synthesised (unsintered) gel, the diffraction profile exhibited a broad hump centered around 2θ value of 22° with no sharp diffraction peaks, indicating an amorphous or poorly crystalline structure. The absence of long-range order confirmed that the gel was primarily composed of an allophane-like hydrated alumino-silicate phase without any other phase. This observation aligned with the FTIR results

https://doi.org/10.38124/ijisrt/25sep1144

presented, which also supported the presence of amorphous alumino-silicate structures.

Upon sintering at 950 °C, sharp and well-defined peaks emerged, corresponding to crystalline mullite phase with minor contributions from corundum-type α -Al₂O₃. Quantitative phase analysis using Rietveld refinement indicated that the sample consisted of approximately 85.2 wt% mullite (JCPDS 15-0776) [20, 23] and 14.8 wt% residual alumina (JCPDS 10-0173). The appearance of mullite at this temperature indicated the onset of the

mullitization reaction, while the persistence of $\alpha\text{-}AlO_3$ suggested incomplete reaction between the silica and alumina phases. Further heat treatment at $1050\,^{\circ}\text{C}$ led to increased crystallinity and phase development [20, 24]. The mullite peaks became sharper and more intense, while $\alpha\text{-}Al_2O_3$ peaks disappeared, indicating the continued incorporation of alumina into the mullite structure. However, new peaks corresponding to crystobalite (C) (JCPDS 39-1425) [25], a high-temperature polymorph of silica, appeared alongside the mullite phase. Rietveld analysis revealed that the sample contained 89.2 wt% mullite and 10.8 wt% crystobalite.

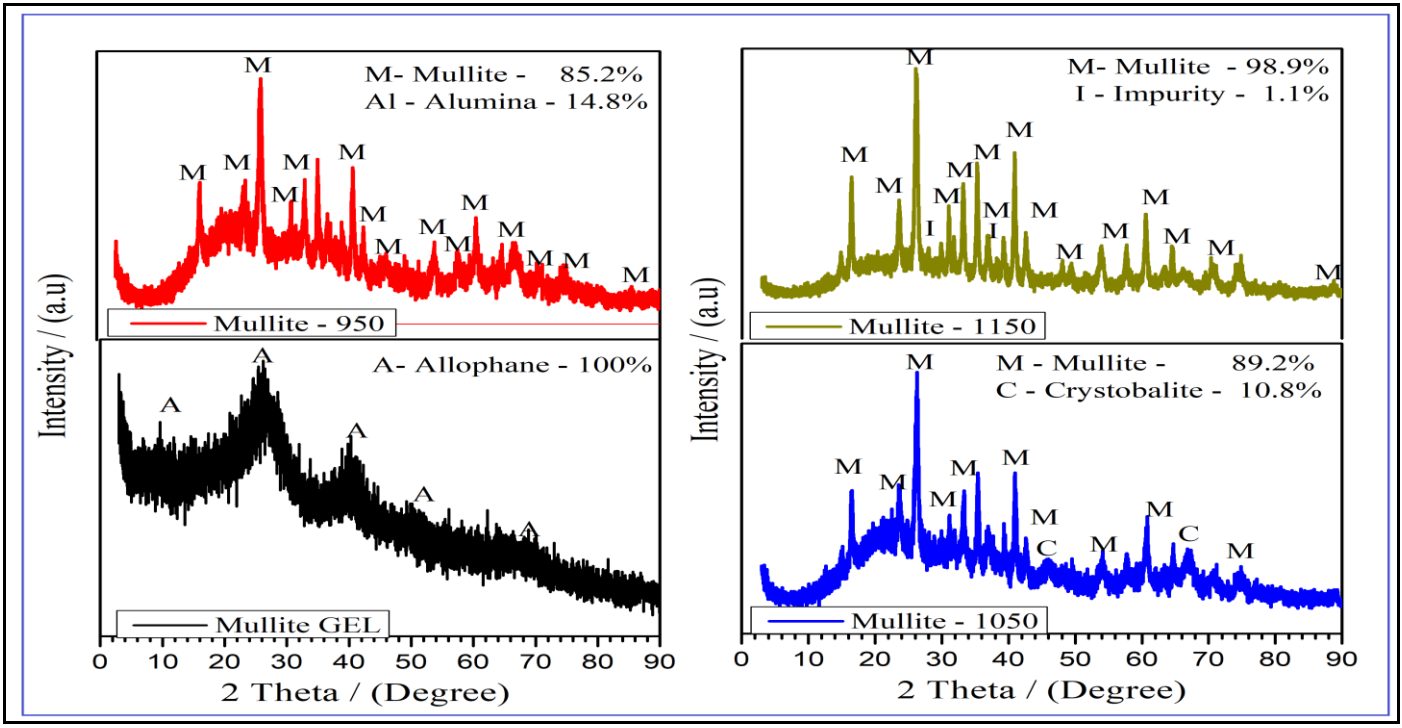


Fig 3 XRD Patterns of Mullite Gel and Sintered Mullite

The presence of crystobalite was attributed to the crystallization of excess free silica not consumed in mullite formation, which is common in silica-rich systems. At the highest sintering temperature of 1150 °C, the XRD pattern showed only sharp, intense mullite peaks, indicating the formation of highly crystalline and nearly phase-pure mullite. Minor background reflections were attributed to less than 1.1 wt% unidentified impurity phases. Rietveld quantification confirmed that the sample consisted of 98.9 wt% mullite, thus making 1150 °C as the optimal temperature for the complete transformation of the gel into crystalline mullite [5,16, 20]. The evolution of crystalline phases as a function

of sintering temperature is summarized in Table 2. The XRD results clearly demonstrated that thermal treatment induced a gradual, but definitive transformation of the precursor gel into crystalline mullite with increasing sintering temperature. The complete disappearance of corundum and crystobalite phases at 1150 °C suggested a near-stoichiometric reaction between silica and alumina precursors, resulting in highly pure mullite. These findings were in good agreement with FTIR spectral features presented in Figure 2, which showed the progressive sharpening of Si–O–Al and Al–O vibrational bands indicative of crystallization.

Table 2 Phase Composition of As-Synthesised Mullite

Sample	Major Phase(s)	Minor Phase(s)	Phase Purity (wt%)		
Mullite Gel	Amorphous (Allophane)	_	100 amorphous		
Mullite – 950 °C	Mullite (M)	α -Al ₂ O ₃ (Al)	85.2 % M, 14.8 % (Al)		
Mullite – 1050 °C	Mullite (M)	Crystobalite (C)	89.2 % M, 10.8 % (C)		
Mullite – 1150 °C	Mullite (M)	Trace impurity (I)	98.9 % M, 1.1 % (I)		

SEM micrographs of the mullite gel and its sintered products shown in Figure 4 elucidate the morphological

evolution of the gel as it underwent structural transformation into crystalline mullite under progressive thermal treatments.

https://doi.org/10.38124/ijisrt/25sep1144

From Figure 4, it can be observed that the SEM image of the mullite gel revealed a highly porous and loosely agglomerated network composed of ultrafine, amorphous particles. The particles lacked distinct boundaries, and the surface appeared rough and irregular, consistent with the poorly crystalline or amorphous nature of the material as previously inferred from XRD and FTIR analyses. This opentextured, sponge-like morphology is typical of sol-gel derived systems and offers a high surface area that is conducive to enhanced solid-state diffusion during subsequent thermal processing [20]. After sintering at 950 °C, the material exhibited evidence of particle coarsening and the early onset of crystallization. While the overall morphology retained significant porosity, emerging faceted grains with sizes ranging from approximately 0.5 to 1 µm were observed, indicating the initiation of mullite and corundum phase formation as confirmed by XRD analysis. The presence of inter-particle necks suggested partial sintering and grain boundary diffusion, though densification remained limited at this stage.

The sample calcined at $1050\,^{\circ}\mathrm{C}$ showed more advanced sintering behaviour. Prominent polygonal grains, typically ranging from 1 to 2 μm in size, were distributed across the surface with a reduced amount of inter-granular porosity. The appearance of plate-like structures and smoother grain boundaries suggested further development of the mullite phase. Residual silica phases, such as crystobalite, likely existed in the matrix as inferred from phase composition data, contributing to the heterogeneous microstructure observed.

At $1150\,^{\circ}$ C, the morphology exhibited significant densification and grain consolidation [4, 23]. The SEM image revealed well-defined, interlocked mullite grains with sizes ranging from 2 to $4\,\mu\text{m}$. The grain surfaces appeared

smoother, and the porosity was markedly reduced, indicating a more complete sintering process. The absence of secondary phase inclusions, such as crystobalite, further confirmed that the mullite phase had become predominant at this stage, in agreement with the XRD results showing nearly 99 % phase purity.

The SEM analyses clearly demonstrated the morphological transition of the precursor gel into a dense mullite ceramic as the sintering temperature increased. A progressive transformation from amorphous, loosely packed nanostructures to well-crystallized, interlocked grains was observed, signifying effective thermal-induced phase development and densification. The correlation between microstructural features and sintering temperature is summarized as follows:

- ➤ Mullite gel: Amorphous, highly porous, and composed of aggregated nano-sized particles.
- ➤ Mullite-950: Initial grain formation and partial sintering, with retained porosity.
- ➤ Mullite-1050: Intermediate densification with grain growth and emergence of crystalline phases.
- ➤ Mullite-1150: Near-complete densification, formation of interlocked crystalline mullite grains, and minimal residual porosity.

These observations confirm that the synthesized mullite gel derived from sodium aluminate and sodium silicate precursors was highly reactive, enabling mullite crystallization at temperatures as low as 950 °C and achieving nearly full densification by 1150 °C. This behaviour presents significant advantages over conventional mullite synthesis methods, which typically require higher sintering temperatures (≥ 1400 °C) to achieve comparable structural evolution.

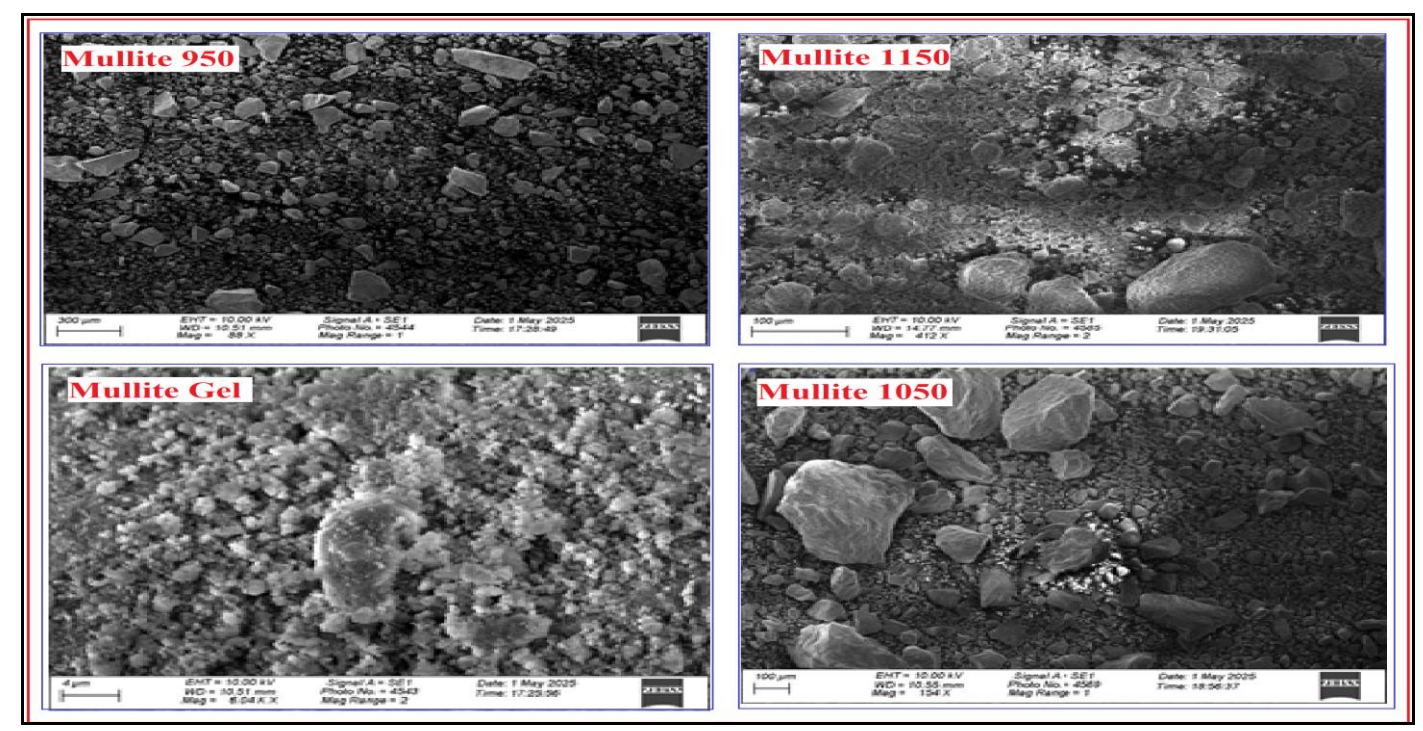


Fig 4 SEM Micrographs of Mullite Gel and Sintered Products

The EDX spectra for all samples presented in Figure 5, revealed the presence of silicon (Si), aluminum (Al), and oxygen (O) as the dominant elements, confirming the expected stoichiometry of mullite. Minor elemental constituents such as sodium (Na) and sulfur (S) were also detected in the precursor mullite gel but showed a progressive decline in intensity with increasing sintering temperature. Even though Carbon (C) was also detected in all samples, it must be emphasized that the carbon signal did not originate from the samples themselves, but rather from the graphite tape used to mount the specimens during EDX analysis. Therefore, variations in carbon content across the samples were not considered chemically relevant and were excluded from interpretive discussion.

Figure 5 shows that the as-prepared mullite gel exhibited significant impurity levels, with Na and S concentrations of 1.6.0 and 2.2 wt% respectively, indicating residual sodium from sodium silicate and sulfur from the precursor sodium aluminate. Upon sintering at 950 °C, a noticeable reduction in these impurities was observed, and by 1050 and 1150 °C, Na and S were either eliminated or reduced below the detection limit, suggesting effective volatilization or diffusion out of the matrix. Furthermore, the increase in aluminum and silicon contents with temperature indicated the formation of a more stoichiometric and homogeneous mullite structure. The decline in oxygen

content above 1050 °C observed in Table 3 below, was consistent with phase densification and crystallization, as reflected in the XRD and FTIR analyses. This evolution in chemical composition summarized in Table 3, shows that the precursor mullite gel contained high oxygen content (~48 wt%) due to its amorphous and hydrated nature, consistent with hydroxylated aluminosilicate species and bound water. Aluminum was the dominant metallic element, with silicon in lower proportion, yielding an Al/Si ratio of ~1.67, slightly above the stoichiometric 3:2 mullite value, likely from incomplete silica incorporation or excess alumina.

Upon sintering at 950 °C, oxygen content decreased slightly (~47.7 wt%), indicating partial dehydroxylation and structural condensation, while the Al/Si ratio dropped, suggesting incorporation of additional silica into the network. At 1050 °C, oxygen content rose (>48 wt%), accompanied by further dehydroxylation and possible formation of a silicarich glass phase, temporarily lowering Al and Si proportions. By 1150 °C, oxygen declined marginally as Al and Si increased, reflecting devitrification of the glassy phase and crystallization of alumina-rich mullite, with the Al/Si ratio approaching the theoretical 3:2 stoichiometry. Overall, the data confirm the compositional evolution of the gel into mullite with increasing temperature, consistent with phase transformations reported in literature [8, 20, 26].

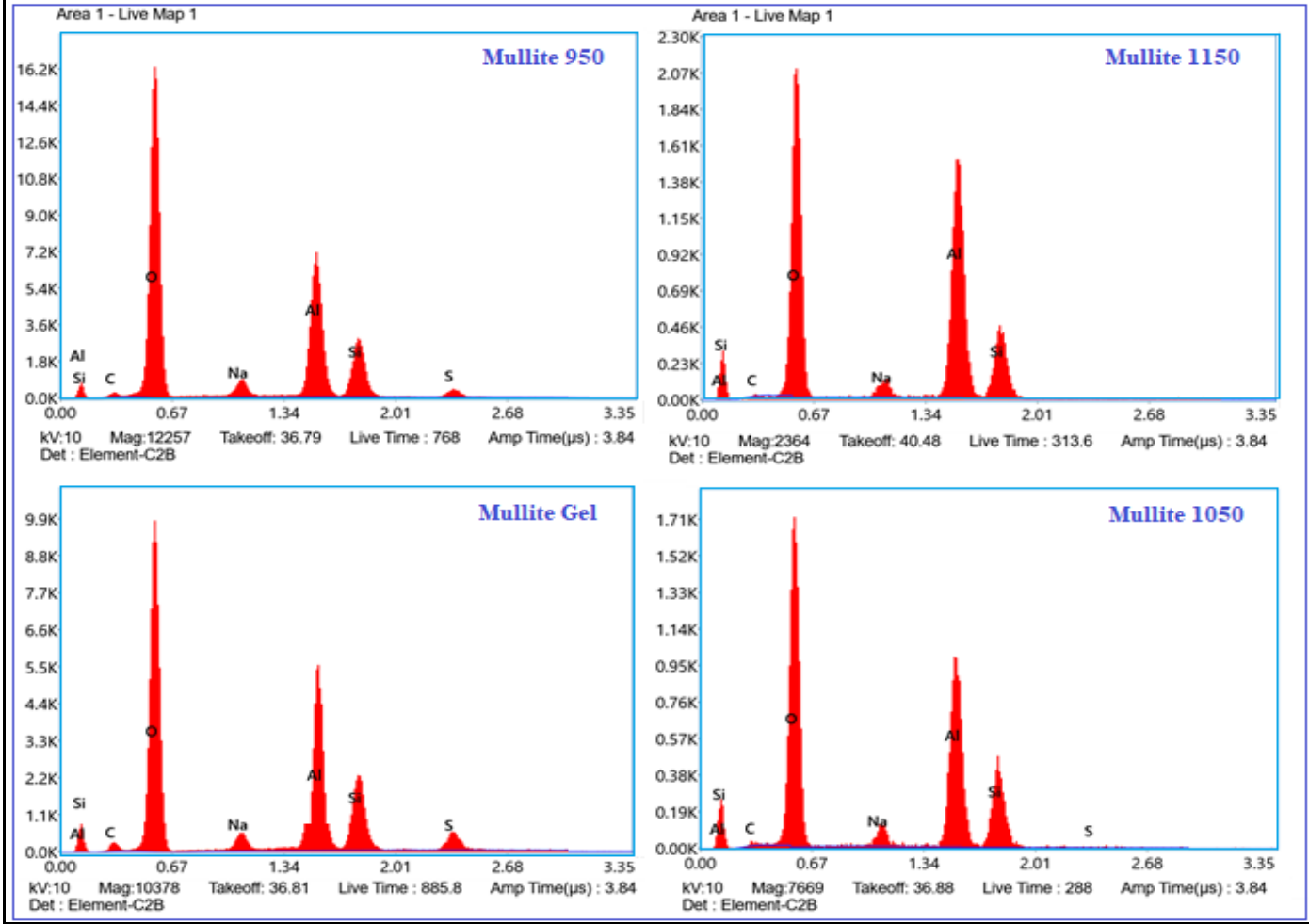


Fig 5 EDX Spectral of Mullite Gel and Its Sintered Products

rusic 5 Elemental Constituents of Mainte Ger and its Sintered Product								
Sample	Elements / wt%							
	Si K	Al K	ОК	Na K	S K	СК		
Mullite Gel	18.31	30.51	48.29	1.60	2.20	2.29		
Mullite 950	18.36	30.63	47.67	0.44	0.62	2.28		
Mullite 1050	18.96	30.70	48.11	0.43	0.02	1.78		
Mullite 1150	19.98	30.69	46.99	0.50	0.00	1.84		

Table 3 Elemental Constituents of Mullite Gel and Its Sintered Product

V. CONCLUSIONS

Mullite was synthesized from an aluminosilicate gel with intentionally high aluminum content, prepared using kaolin-derived sodium aluminate and sodium silicate. XRD analysis showed that complete transformation of the aluminosilicate gel into mullite with approximately 99.0 % phase purity was achieved at 1150 °C, while elemental analysis confirmed dehydroxylation, sulfur elimination, minor sodium retention, and convergence of the Al/Si ratio towards the theoretical 3:2 value. These findings demonstrated that precise control of aluminosilicate gel formation, combined with optimization of sintering temperature, is critical for obtaining high-purity mullite from the kaolin-derived precursors.

ACKNOWLEDGMENT

Authors would like to express their profound gratitude to ZEOTEC LTD, Ghana for funding this research work.

REFERENCES

- [1]. José, V., Pires, E., Almeida, D., Patrício, W., Borges, R., Araújo, G. De, & Lucena, H. De. (2018). Mineralogical and dielectric properties of mullite and cordierite ceramics produced using wastes. *Ceramics International*, 45(4), 4692–4699.
- [2]. Krenzel, T. F., Schreuer, J., Laubner, D., Cichocki, M., & Schneider, H. (2019). Thermo-mechanical Properties of Mullite Ceramics: New data. *Journal of American Ceramic Society*, 102(6), 416–426. https://doi.org/10.1111/jace.15925
- [3]. Lima, L. K. S., Silva, K. R., Menezes, R. R., Santana, L. N. L., & Lira, H. L. (2022). Microstructural characteristics, properties, synthesis and applications of mullite: a review. *Ceramica*, 68(6), 126–142. https://doi.org/10.1590/0366-69132022683853184.
- [4]. Mahnicka-goremikina, L., Svinka, R., Svinka, V., Grase, L., Juhnevica, I., Rundans, M., ... Fomenko, S. (2022). Thermal Properties of Porous Mullite Ceramics Modified with. *Materials*, *15*(10), 7935. https://doi.org/10.3390/ma15227935.
- [5]. Schneider, H., Schreuer, J., & Hildmann, B. (2008). Structure and properties of mullite — A review. *Journal of the European Ceramic Society*, 28(5), 329–344. https://doi.org/10.1016/j.jeurceramsoc.2007.03.017.
- [6]. Sultana, P., Das, S., Bhattacharya, A., Basu, R., & Nandy, P. (2011). Mullite formation in coal fly ash is facilitated by the incorporation of magnesium oxide. *Rev. Adv. Mater. Sci*, 27, 69-74.

- [7]. Romero, M., Padilla, I., Contreras, M., & Aurora, L. (2021). Mullite-Based Ceramics from Mining Waste: A Review. *Minerals*, 11(332), 1–39. https://doi.org/10.3390/min11030332.
- [8]. Shishavan, N. M., ESlami-Farsani, R., Ebrahimnezhad-Kaljiri, H., & Aghamohammadi, H. (2019). The effects of pre-heating and sintering temperature on the sol-gel synthesis of mullite nanoparticles. *Materials Research Express*, 6(10), 105045. https://doi.org/10.1088/2053-1591/ab3929.
- [9]. Tabit, K., Borja, W., & Saadi, L. (2021). naturally occurring andalusite and marble waste Low-temperature synthesis of mullite-based ceramics from Moroccan naturally occurring andalusite and marble waste. *International Journal of Applied Ceramic Technology*, 19(3), 1274–1280. https://doi.org/10.1111/ijac.13942.
- [10]. Jurado, L. T., Hernández, R. M. A., & Rocha-Rangel, E. (2013). Sol-Gel Synthesis of Mullite Starting from Different Inorganic Precursors. *Journal of Powder Technology*, 2013(1), 268070. https://doi.org/10.1155/2013/268070.
- [11]. Komarneni, S., Schneider, H., & K. Okada. (2005). Mullite Synthesis and Processing. In *Mullite* (Vol. 10, pp. 251–348). Weinheim: Wiley VCH Verlag GmbH & Co.
- [12]. EL-Rafei, A. M., & Mansour, T. S. (2023). Physico-Mechanical and Microstructure Characteristics of Porous Mullite Creamics. *Silicon*, 15(6), 7157–7170. https://doi.org/10.1007/s12633-023-02527-y.
- [13]. Cividanes, L. S., & Campos, T. M. B. (2010). Review of mullite synthesis routes by sol gel method. *Journal of Sol-Gel Science Technology*, *55*(1), 111–125. https://doi.org/10.1007/s10971-010-2222-9.
- [14]. Chargui, F., Hamidouche, M., Belhouchet, H., Jorand, Y., Doufnoune, R., & Fantozzi, G. (2018). Mullite fabrication from natural kaolin. *Boletín de La Sociedad Española de Cerámica y Vidrio*, *57*(4), 169–177. https://doi.org/10.1016/j.bsecv.2018.01.001.
- [15]. Oluseyi, A. K., Aladesuyi, O., & Pal, M. (2016). Evaluation of Nigerian Source of Kaolin as a Raw Material for Mullite Synthesis. *Oriental Journal of Chemistry*, 32(3), 1571–1582. https://doi.org/10.13005/ojc/320333.
- [16]. Sanchez-Soto, P. J., Eliche-quesada, D., Martinez-Martinez, S., Perez-Villarejo, L., & Garzon, E. (2022). Study of a Waste Kaolin as Raw Material for Mullite Ceramics and Mullite Refractories by Reaction Sintering. *Materials*, *15*(1), 1–22. https://doi.org/10.3390/ma15020583.

- [17]. Val, M., & Blah, V. (2021). Effects of Kaolin Additives in Fly Ash on Sintering and Properties of Mullite Ceramics. *Minerals*, 11(8), 887.
- [18]. Al-sagheer, N. A., Aboulfotouh, G., Abdel, N. F., & Hashem, F. S. (2024). Extraction of silicon oxide from the partially dealuminated metakaolin residue of the kaolin-based aluminum sulfate manufacturing process. *Egyptian Journal of Petroleum*, *33*(1), 567–576. https://doi.org/10.62593/2090-2468.1051.
- [19]. Tijani, J. O., Bankole, M. T., Hussein, A., Oketoye, J. A., & Abdulkareem, A. S. (2019). Influence of Synthesis Parameters in the Preparation of Silicon (IV) Oxide Nanoparticles from Dealuminated Metakaolin and Metakaolin with Na2SiO3. *Journal of Chemical Society of Nigeria*, 44(6), 1143–1156.
- [20]. Jana, A., & Ray, D. (2020). Synthesis and characterization of sol-gel derived monophasic mullite powder. *Ceramica*, 66(3), 307–313.
- [21]. Aripin, H., Mitsudo, S., Prima, E. S., Sudiana, I. N., Kikuchi, H., Sano, S., & Sabchevski, S. (2015). Crystalline mullite formation from mixtures of alumina and a novel material silica xerogel converted from sago waste ash. *Ceramics International*, 4(5), 6488–6497. https://doi.org/10.1016/j.ceramint.2015.01.092.
- [22]. Okada, K. (2008). Activation energy of mullitization from various starting materials. *Journal of the European Ceramic Society*, 28(5), 377–382. https://doi.org/10.1016/j.jeurceramsoc.2007.03.015.
- [23]. Alves, H. P., Silva, J. B., Campos, L. F., Torres, S. M., Dutra, R. P., & Macedo, D. A. (2016). Preparation of mullite based ceramics from clay–kaolin waste mixtures. *Ceramics international*, 42(16), 19086-19090.
 - http://dx.doi.org/10.1016/j.ceramint.2016.09.068.
- [24]. Viswanath, B., Darshankumar, J., Gunapriya, B., Karthi, M., Sankaramoorthy, T., & Murugesan, K. (2022, November). Preparation and characterization of mullite ceramic nano powder for use in nanocomposites. In AIP Conference Proceedings (Vol. 2446, No. 1, p. 120001). AIP Publishing LLC.
- [25]. Fernandes, L., de Carvalho, R. A., Amaral, A. C., Pecoraro, E., Salomão, R., & Trovatti, E. (2019). Mullite cytotoxicity and cell adhesion studies. *Journal* of Materials Research and Technology, 8(3), 2565-2572
- [26]. Fang, J., Yan, B., & Deng, T. (2019). Fast transformation of andalusite into mullite by addition of yttria. *Boletín de la Sociedad Española de Cerámica y Vidrio*, 58(4), 142-150.